An image-based notion for therapeutic planar organ activity dosimetry in a developing country: Masterdose software

Bronwin Van Wyk[1] **MSc,**
Francis Hasford[2] **PhD,**
Nozipho Nyakale[3] **MD,**
Mboyo-Di-Tamba Vangu[4] **MD, PhD**

1.Sefako Makgatho University, Department of Medical Physics, Pretoria, South Africa
2. University of Ghana, School of Nuclear and Allied Sciences, Department of Medical Physics, Accra, Ghana
3.Sefako Makgatho University, Department of Nuclear Medicine, Pretoria, South Africa
4. Witwatersrand University, Department of Nuclear Medicine, Johannesburg, South Africa

Keywords: Software - Planar - Dosimetry - Quantification - Masterdose

Corresponding author:
Bronwin Van Wyk BMedSc Hons, MSc,
SefakoMakgatho University,
Department of Medical Physics,
Pretoria, South Africa
Tel: +27125214771,
Fax: +27125214384
bronwin.vanwyk@smu.ac.za

Received:
1 December 2021
Accepted revised:
7 April 2022

Abstract

Objective: Planar dosimetry is often performed in developing countries due to its simplicity during basic quantitative dosimetry. The geometric mean method is often used during planar dosimetry and imaging counts can be corrected for background, attenuation and scatter. The aim of our study was to develop computerized software called Masterdose that may be used for therapeutic isotope planar organ personalized dosimetry. **Materials and Methods:** Masterdose software uses various methods to correct for background, scatter and attenuation. We also introduced a method to convert imaging counts to activity on the software, which is Java based and runs on Windows, Linux and Macintosh platforms. **Results:** Three user interfaces named image processing, quantification and dosimetry were developed for the software. Masterdose could quantify kidney and liver doses of lutetium-177-DOTA-0-Tyr3-octreotate (^{177}Lu-DOTATATE) patients. The software was validated through calculation of the kidney and liver doses of ten neuroendocrine tumour patients (NET) treated with ^{177}Lu-DOTATATE. **Conclusion:** Masterdose presents an option for planar quantification that can be used as a quality control tool to verify imaging counts and perform dosimetry in particular organs.

Hell J Nucl Med 2022; 25(1): 71-82 *Published online: 30 April 2022*

Introduction

Planar whole-body imaging is carried out by translating the patient and bed in the z-direction between an opposed dual head gamma camera, in the anterior and posterior position [1]. These planar whole-body images are degraded by factors like background, attenuation and scatter which limit the quantitative ability of this modality. These factors occur due to the interaction of emitted photons with tissue before the photons are detected externally by the gamma camera. Attenuation describes the reduction in detected photons due to interactions such as photoelectric absorption or Compton scatter [2]. This interaction probability depends on the photon energy, material composition and the amount of material [2]. Compensation is usually applied to correct for artifacts during patient imaging by accounting for fewer counts due to attenuation [3].

Planar quantification using scintillation camera imaging and conjugated views remain the most widely used method for attenuation correction [3, 4]. During this method, a geometric mean (GM) of the count rate is calculated with two opposed scintillation camera images. The measured count rates in the GM method depends on attenuation between the two views and not the source depth. In planar imaging, source depth in the direction parallel to the projection is not resolved. This complicates activity quantification, as more than one organ can contribute to a particular pixel value in the projection image. Therefore, the GM method is theoretically independent of the source depth and gives "reasonable" dose estimates for large organs without position overlap and background activity [5,6]. However, this method generally reduces the image contrast and the detectability for small lesions.

Several researchers have developed in-house computational software for radionuclide quantification in Nuclear Medicine. Example, in the study of Li et al. (2020) [7], they developed a comprehensive 3D dosimetric software, BIGDOSE, with new features of image registration and virtual computed tomography (CT) for patient-specific dosimetry. The software produced organ dose errors of -9.59%±9.06%, -8.36±5.82%, -23.41%±6.67% and -6.05%±2.06% for liver, spleen, kidneys and lungs, while OLINDA/EXM comparatively produced -25.72%±12.52%, -14.93%±10.91%, -28.63%±12.97% and -45.30%± 5.84% respectively. In recent studies, more research and commercial dosimetric software

have been developed. These include HERMES® [8], RAYDOSE [9], PLANET® [10], OEDIPE [11], VoxelMed [12], VRAK [13], JADA [14], STRATOS® [15], and VIDA [16]. Ramos et al. (2017) [17] have reviewed several of these software codes for internal dosimetry. The aim of our study was to put forward a notion for therapeutic isotope planar organ personalized dosimetry using computerized software from the perspective of a developing country.

Materials and Methods

Masterdose development

Masterdose was written in Java (Sun Microsystems) programming language. User interfaces (UI) were developed using JavaFX, which is the latest version for desktop applications. Three UI were designed for image processing, quantification and dosimetry, as indicated in the theoretical framework design (Figure 1). The software was designed using a java programme based on upgraded Image J software. The underlying framework from Image J was used to zoom images and retrieve counts. Counts were acquired by drawing organ region of interest (ROI) on planar images at different time intervals. Background counts were generated by drawing ROI around general activity update on patient images.

The quantification user interface was developed from written algorithm for counts of activity to radionuclide activity conversion (Figure 2).

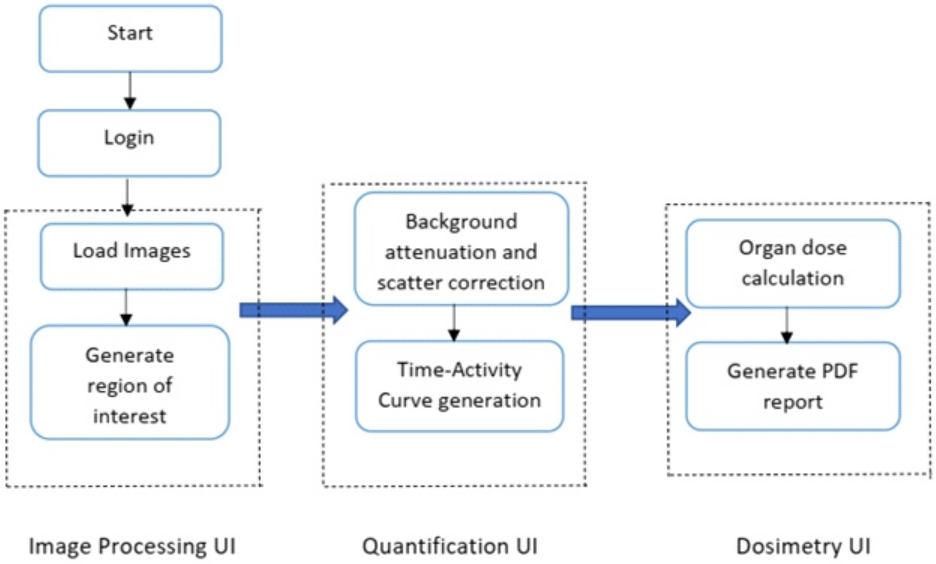

Figure 1. Theoretical framework design of Masterdose software.

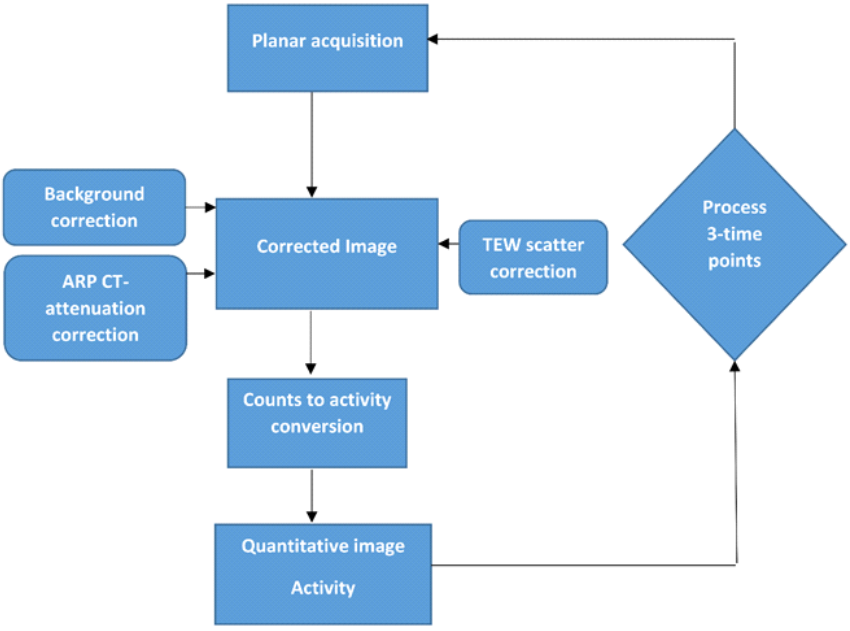

Figure 2. Masterdose quantification.

The authors developed the software to correct for background, attenuation and scatter counts. All planar images were acquired using the GM method on a dual headed Philips Marconi Meridian gamma camera (New York, USA). This gamma camera did not have a CT component that could be used for attenuation correction. To overcome the shortcoming, authors determined a "generic attenuation correction factor" (gACF) using a 70keV transmission energy and 20mAs scout scan of an anthropomorphic Alderson Rando Phantom (ARP), demonstrated (Figure 3). Scan image was presented in 256× 256 matrix.

The torso of the ARP had horizontally transacted with 2.5cm thick slices and was used to mimic a patient [18]. Each region of the ARP had holes, which were plugged with bone-equivalent, soft-tissue-equivalent and lung-tissue-equivalent pins that resemble the human body. The dimensions of the regions are given (Table 1).

Table 1. *Dimensions of the torso region of anthropomorphic phantom.*

ARP Torso	Dimensions (mm^3)
Region 1	300 × 100 × 180
Region 2	300 × 100 × 220
Region 3	300 × 100 × 200

The skeletons of the ARP were polymer mouldings; which reproduced the shape, mass density and attenuation coefficients of cortical bone. The lungs were moulded from syntactic foam, with a specific density of 0.30g/cm^3 [18]. Equation (1) was used to determine the gACF.

$$gACF = ln\frac{I_{det}}{I_x} = \sum u_i \Delta x_i \qquad (1)$$

where,

I_x = transmission for a patient thickness
I_{det} = counts on the detector
μ = attenuation coefficient for different materials
x_i = different patient thicknesses

Scatter corrections were performed using the triple-energy window(TEW) technique demonstrated in Equation (2).

$$I_{scatter} = \left(\frac{I_{lower}}{W_{lower}} + \frac{I_{upper}}{W_{upper}}\right) x \frac{W_{peak}}{2} \qquad (2)$$

where,

$I_{scatter}$ is the scatter estimate,
I_{lower} and I_{upper} are the scatter counts from lower and upper energy windows respectively,
and $W_{lower,}$ W_{upper} and W_{peak} are the window widths of the lower, upper and peak windows respectively.

The scatter correction method, had two auxiliary energy windows, one above and the other just below the photopeak energy window [19]. The scatter in the photopeak was then estimated using a trapezoidal approximation. The position and width of the energy windows were carefully selected.

Radionuclide quantification and dose evaluation

The kidney doses of ten patients that underwent peptide therapy using lutetium-177-DOTA-0-Tyr3-octreotate (^{177}Lu-DOTA-TATE) were calculated using the developed Masterdose software. The patients were classified using the Eastern Cooperative Oncology Group (ECOG) system to assess the patient performance status (Table 2).

Scintigraphic DICOM images of the patients were retrieved and imported into Masterdose for the dose estimations. The patients used in this study generally had advance disease, as demonstrated by the example (Figure 4).

"Counts to activity" correction was performed using a 5mL syringe with a 37MBq ^{177}Lu prepared in a petri dish. The camera heads were set to "H-mode acquisition" with the petri dish suspended 10cm above the collimator as demonstrated (Figure 5).

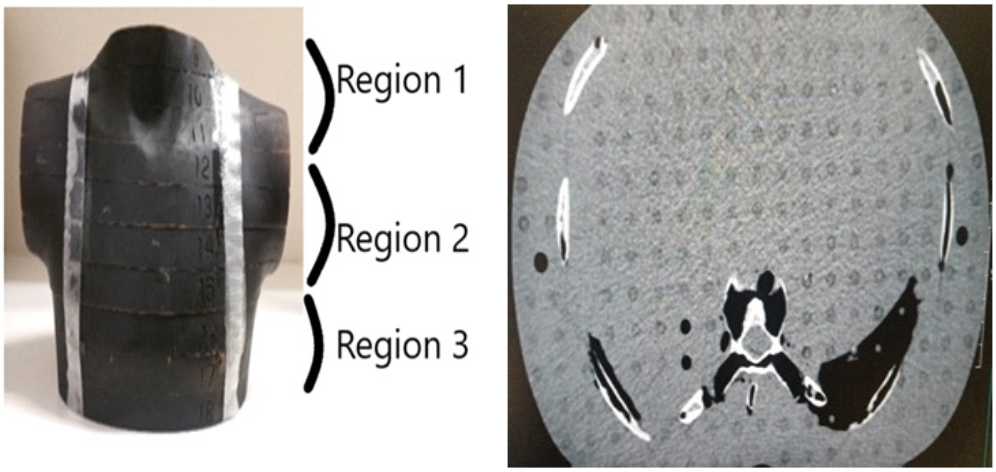

Figure 3. ARP phantom used to determine a gACF

Table 2. *ECOG classification of patient performance status.*

Grade	ECOG classification
0	Fully active, able to carry on all pre-disease performance without restriction
1	Restricted in physically strenuous activity but ambulatory and able to carry out work of a light or sedentary nature, e.g., light house work, office work
2	Ambulatory and capable of all self-care but unable to carry out any work activities. Up and about more than 50% of waking hours
3	Capable of only limited self-care, confined to bed or chair more than 50% of waking hours
4	Completely disabled. Cannot carry on any self-care. Totally confined to bed or chair
5	Dead

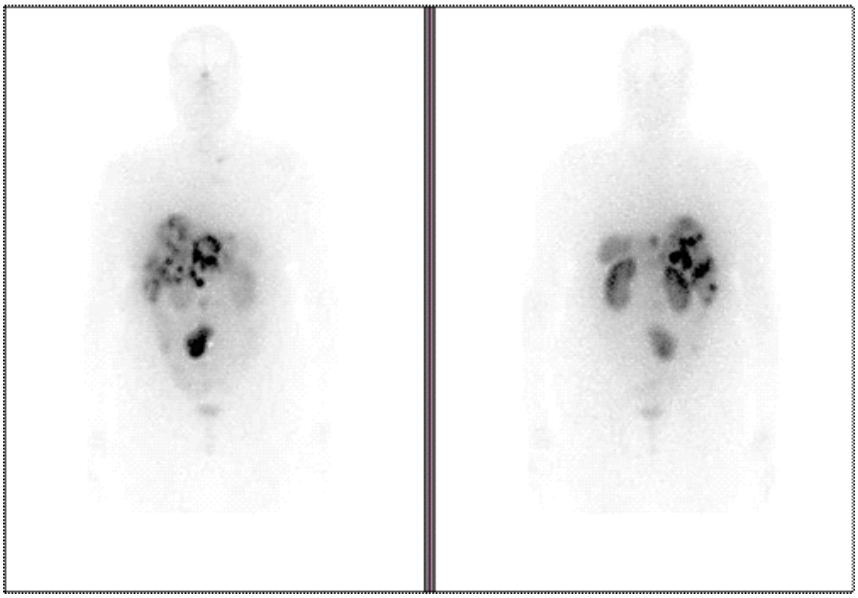

Figure 4. Whole body images of a patient with advanced liver disease.

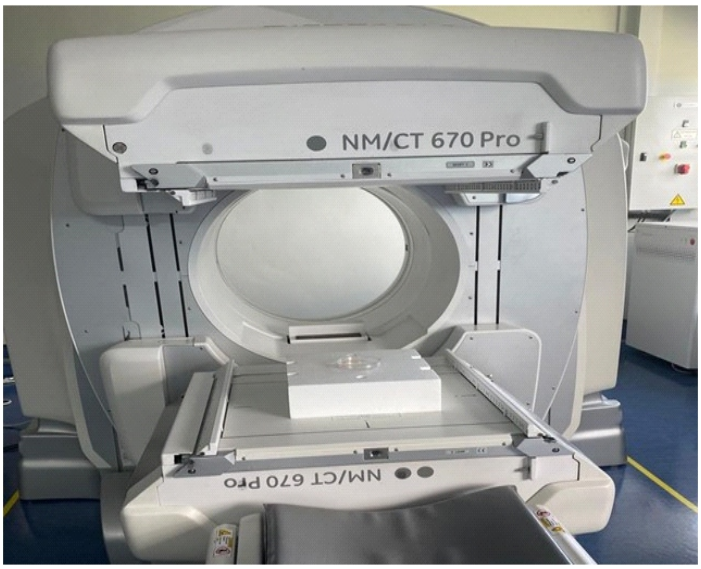

Figure 5. Demonstration of the ^{177}Lu acquisition in a petri dish.

Background images were then acquired with no source in place near the gamma cameras for the same number of counts. Four million counts were then acquired with a 15 percent (%) energy window width. Radionuclide counts were converted to activity using Equation 3 [20].

$$Counts\ to\ Activity = \frac{1}{A_{cal}}\left[C_{10} \times \exp\left(\frac{T_{10} - T_{cal}}{T_{half}}\ln 2\right) \times \left(\frac{\ln 2}{T_{half}}\right)\left(1 - \exp\left(-\frac{T_{acq}}{T_{half}}\ln 2\right)\right)^{-1}\right] \quad (3)$$

where,

A_{cal} is the radionuclide activity in the petri dish,
C_{10} is the counting rate derived from the reconstructed image (counts/dwell time),
T_{10} is the start time at 10 cm,
T_{acq} is the duration of the acquisition at 10 cm,
T_{cal} is the time of activity calibration,
T_{half} is half-life of ^{177}Lu

Masterdose software was designed to generate a time activity curve. The area under the curve was determined using the trapezoidal method shown in Equation (4) to generate the accumulated count in the organ.

$$Cumulated\ counts = \sum\left(\frac{y1 + y2}{2}\right) \times (x2 - x1) \quad (4)$$

The organ dose on the Masterdose software was calculated through Equation (5), multiplying the accumulated count with "S-values". The "S-values" on the Masterdose software were obtained from Organ Level Internal Dose Assessment/EX-ponential Modeling (OLINDA/EXM) software [27], which included 10 whole-body phantoms.

$$D = \sum Cumulated\ counts \times s - value \quad (5)$$

The "S-values" were corrected for the mass of the organ as demonstrated in Equation (6).

$$s - value = self/cross\ dose\ s - value\ x\ \frac{mass\ s - value}{mass\ phantom} \quad (6)$$

Masterdose software was designed to generate a full PDF dosimetry report. The report was generated using iText framework. J Charts was used to create the charts on the screen.

Results

Masterdose has capability to quantify counts of activity for each acquired image, which plays an important role in patient dosimetry [21-23]. The software corrects for background counts, attenuation and scatter during image quantification. Table 3 gives the results obtained for the *gAFC* used on Masterdose.

Table 3. *Determined gAFC from the average ACF from anthropomorphic phantom.*

ARP Torso	Dimensions (mm^3)	ACF
Region 1	300 × 100 × 180	2.00
Region 2	300 × 100 × 220	3.11
Region 3	300 × 100 × 200	2.88
	gAFC	**2.66**

The photon energy spectrum of 70keV, used to obtain the results in (Table 3), was similar to a study by Minarik et al. (2005) [24]. For this energy spectrum, the differences between the mass attenuation coefficients of various soft tissues are small, since the dominant photon interaction process was Compton scattering. Other studies have also shown similar results [25, 26], mass attenuation coefficients were equal for both lung and soft tissue. Linear attenuation coefficient differences were governed by the difference in mass densities. This study therefore endorses the use of the *gAFC* for attenuation correction in a gamma camera without a CT component.

The ten patients whose data were considered in this study had NET condition of the adrenal gland, liver, endocrine and lung. The ^{177}Lu-DOTATATE patient data, including gender, NET site and ECOG is given (Table 4).

Table 4. *Data of NETs patients treated with ^{177}Lu-DOTATATE.*

ID	Gender (M/F)	NET site	ECOG
1	F	Adrenal gland	0
2	F	Liver	0
3	F	Endocrine unspecified	2
4	M	Right lung	0
5	F	Left lung	0
6	M	Liver	0
7	F	Liver	2
8	M	Pancreas	2
9	M	Liver	2
10	F	Liver	0

The photopeak of interest used in this study for the TEW technique was the main photopeak of ^{177}Lu, 208keV, as this was the main energy peak used often for image quantification [21]. The main energy window was therefore, 192.4keV to 223.6keV with a width of 31.2keV. The lower energy window was 177.97 keV to 192.4keV with a width of 14.43keV. The upper energy window was 223keV to 240.37keV with a width of 16.77keV. The TEW counts generated for the ten ^{177}Lu-DOTATATE patient cases are given (Table 5).

Table 5. *TEW counts generated on Masterdose for the 10 patients.*

Parameter		Quantity
Number of patients		10
TEW counts	Minimum	4102
	Maximum	4139
	Mean (±SD)	4122 (±12)

Once the counts were corrected for attenuation and scatter, the resultant counts were converted to activity. The software subtracts all scattered counts from the background corrected quantified count and multiplies the attenuation corrected counts. The corrected counts obtained were then divided by "counts to activity" conversion factor.

The factor used to convert "counts to activity" for the ^{177}Lu patients in our study was 6.5 counts per second per Mbq through Equation (3). All imaging were performed with medium energy collimators and planar energy window settings. "Counts to activity" obtained on the Philips Marconi Meridian gamma camera were comparable to the manufacturer's specifications [28].

The Masterdose user interface homepage is demonstrated (Figure 6), allowing for patient identification and graphical demonstration of image counts uptake in a particular organ.

Numerical example of the trapezoidal modelling of kidney is demonstrated (Table 6).

Table 6. *Trapezoidal modelling for the liver.*

Parameter		Kidneys	Liver
Number of patients		10	
Accumulated Activity (MBq.h)	Minimum	11072	22717
	Maximum	17510	42816
	Mean	14301	32812

Estimated doses to the kidneys and liver for the ten patients on the Masterdose software are given (Figure7).

The administered ^{177}Lu primarily secretes through the kidneys as seen from the scintigram (Figure 4) and in the estimated doses reported (Figure 7). This makes the kidneys the dose-limiting organs when treating tumours with ^{177}Lu-DOTATATE. To counter act and reduce the high kidney retention, a positively charged amino acid, L-lysine was co-infused to competitively inhibit the proximal tubular reabsorption of

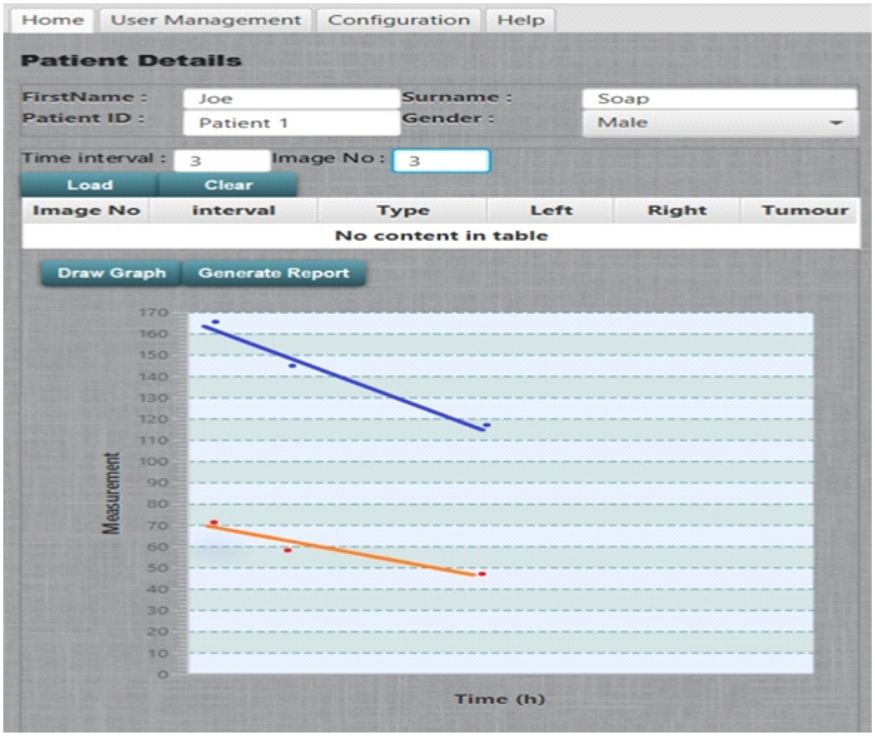

Figure 6. Home page of Masterdose software user interface demonstrating Patient number 1 data. Blue-Kidney, Orange-Liver.

the ^{177}Lu-DOTATATE. The co-administration of amino acid led to significant reduction in the renal absorbed dose for our study.

Sample of the Masterdose generated report is given (Figure 8).

The S-values and mass conversion factors used for the dose estimation of the kidneys and liver are given (Figures 9-12).

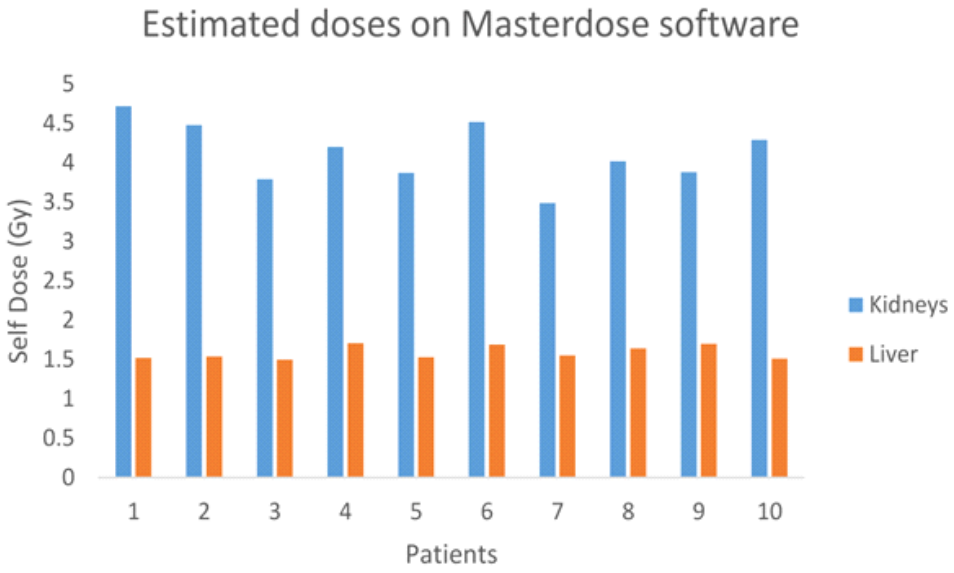

Figure 7. Estimated doses on Masterdose.

Medical Scan Report

Study Name	**Peptide Radiotherapy Cycle 1**
Patient Name	**Joe**
Patient Surname	**Soap**
Radionuclide	**^{177}Lu-DOTATATE**
Date	**07/06/2020**
Kidney Dose	**4.72 Gy**
Liver Dose	**1.52 Gy**

Figure 8. Generated report from Masterdose showing patient dose data.

	Adrenals	Brain	Breasts	GB Cont	LLI Cont	SI Cont	StomCont	ULI Cont	HeartCon	Hrt Wall	Kidneys	Liver	Lungs	Muscle	Ovaries	Pancreas	Red Mar.	CortBone	TrabBone	CortBone	TrabBone	Spleen	Testes	Thymus	Thyroid	UB Cont	Uterus	TotBody
Adrenals	1.46E-03	1.39E-10	1.35E-08	8.58E-08	6.60E-09	1.97E-08	7.50E-08	2.42E-08	6.88E-08	7.66E-08	2.01E-07	1.22E-07	6.38E-08	3.11E-08	9.92E-09	3.00E-07	6.74E-08	2.99E-08	2.99E-08	2.99E-08	2.99E-08	1.26E-07	5.20E-10	1.61E-08	2.24E-09	2.74E-09	5.88E-09	3.57E-07
Brain	1.39E-10	1.73E-05	9.72E-10	5.81E-11	6.70E-12	1.60E-11	1.78E-10	1.89E-11	1.01E-09	8.55E-10	5.71E-11	2.65E-10	2.24E-09	6.15E-09	6.67E-12	1.62E-10	2.30E-08	3.34E-08	3.34E-08	3.34E-08	3.34E-08	2.24E-10	7.62E-13	2.19E-09	3.69E-08	2.78E-12	5.77E-12	3.45E-07
Breasts	1.35E-08	9.72E-10	6.84E-05	8.69E-09	7.68E-10	2.24E-09	1.55E-08	2.50E-09	6.83E-08	7.44E-08	5.70E-09	1.91E-08	6.48E-08	1.20E-08	7.94E-10	1.69E-08	1.47E-08	8.91E-09	8.91E-09	8.91E-09	8.91E-09	1.25E-08	0.00E+00	6.75E-08	8.01E-09	4.45E-10	8.95E-10	3.39E-07
Gallbladder Wall	9.31E-08	5.68E-11	9.19E-09	2.15E-04	1.67E-08	1.19E-07	8.20E-08	2.08E-07	2.71E-08	3.17E-08	1.08E-07	2.41E-07	2.02E-08	3.28E-08	2.76E-08	2.15E-07	3.09E-08	1.20E-08	1.20E-08	1.20E-08	1.20E-08	3.43E-08	2.09E-09	7.62E-09	8.59E-10	1.00E-08	3.06E-08	3.59E-07
LLI Wall	5.95E-09	5.71E-12	8.08E-10	1.49E-08	8.35E-05	1.62E-07	2.40E-08	5.93E-08	1.26E-09	1.54E-09	1.50E-08	4.06E-09	1.01E-09	3.68E-08	3.12E-07	1.17E-08	5.51E-08	2.02E-08	2.02E-08	2.02E-08	2.02E-08	1.23E-08	5.47E-08	5.27E-10	7.88E-11	1.60E-07	1.36E-07	3.58E-07
Small Intestine	1.97E-08	1.60E-11	2.24E-09	1.25E-07	2.00E-07	2.82E-05	5.48E-08	3.49E-07	4.31E-09	5.69E-09	5.77E-08	3.14E-08	3.76E-09	3.08E-08	2.54E-07	3.77E-08	5.04E-08	1.57E-08	1.57E-08	1.57E-08	1.57E-08	2.70E-08	7.00E-09	1.48E-09	1.55E-10	5.88E-08	2.30E-07	3.59E-07
Stomach Wall	7.58E-08	9.23E-11	1.62E-08	8.03E-08	3.47E-08	5.82E-08	4.64E-05	7.79E-08	4.54E-08	7.13E-08	6.93E-08	3.98E-08	3.22E-08	2.99E-08	1.55E-08	3.50E-07	2.25E-08	1.09E-08	1.09E-08	1.09E-08	1.09E-08	2.12E-07	1.46E-09	9.72E-09	1.30E-09	6.08E-09	1.47E-08	3.55E-07
ULI Wall	2.35E-08	1.93E-11	2.27E-09	2.13E-07	8.35E-08	3.78E-07	7.17E-08	5.17E-05	6.18E-09	7.71E-09	5.77E-08	5.05E-08	5.02E-09	3.03E-08	2.28E-07	4.42E-08	4.26E-08	1.38E-08	1.38E-08	1.38E-08	1.38E-08	2.82E-08	5.22E-09	1.74E-09	2.72E-10	4.30E-08	1.13E-07	3.58E-07
Heart Wall	7.66E-08	8.55E-10	7.44E-08	2.75E-08	1.67E-09	5.69E-09	6.43E-08	8.21E-09	2.68E-05	7.58E-05	2.12E-08	6.41E-08	1.21E-07	2.53E-08	2.01E-09	9.56E-08	2.97E-08	1.57E-08	1.57E-08	1.57E-08	1.57E-08	4.39E-08	2.23E-10	2.04E-07	1.14E-08	6.50E-10	1.81E-09	3.55E-07
Kidneys	2.01E-07	5.71E-11	5.70E-09	1.03E-07	1.93E-08	5.77E-08	7.42E-08	5.72E-08	1.71E-08	2.12E-08	8.03E-05	8.13E-08	1.80E-08	2.73E-08	1.89E-08	1.37E-07	4.71E-08	1.73E-08	1.73E-08	1.73E-08	1.73E-08	1.85E-07	1.05E-09	5.08E-09	1.06E-09	6.04E-09	1.72E-08	3.53E-07
Liver	1.22E-07	2.65E-10	1.91E-08	2.25E-07	4.94E-09	3.14E-08	3.97E-08	5.07E-08	5.81E-08	6.41E-08	8.13E-08	1.29E-05	5.47E-08	2.09E-08	1.03E-08	1.06E-07	2.45E-08	1.34E-08	1.34E-08	1.34E-08	1.34E-08	1.97E-08	5.30E-10	1.61E-08	2.60E-09	3.47E-09	8.99E-09	3.54E-07
Lungs	6.43E-08	2.25E-09	6.52E-08	1.86E-08	1.42E-09	3.77E-09	2.97E-08	4.70E-09	1.28E-07	1.22E-07	1.81E-08	5.63E-08	2.39E-05	2.61E-08	1.75E-09	4.67E-08	3.05E-08	1.85E-08	1.85E-08	1.85E-08	1.85E-08	4.57E-08	1.35E-10	7.95E-08	2.37E-08	3.26E-10	1.30E-09	3.50E-07
Muscle	3.11E-08	6.15E-09	1.20E-08	3.16E-08	3.38E-08	3.08E-08	2.77E-08	2.93E-08	2.45E-08	2.53E-08	2.73E-08	2.09E-08	2.59E-08	8.72E-07	3.93E-08	3.42E-08	2.53E-08	2.08E-08	2.08E-08	2.08E-08	2.08E-08	2.87E-08	2.77E-08	2.94E-08	3.24E-08	3.59E-08	3.94E-08	3.47E-07
Ovaries	9.92E-09	6.67E-12	7.94E-10	2.84E-08	3.51E-07	2.54E-07	1.54E-08	2.11E-07	1.49E-09	2.01E-09	1.89E-08	1.03E-08	1.75E-09	3.93E-08	2.72E-03	1.06E-08	5.78E-08	1.80E-08	1.80E-08	1.80E-08	1.80E-08	1.06E-08	0.00E+00	6.56E-10	8.84E-11	1.45E-07	4.21E-07	3.61E-07
Pancreas	3.00E-07	1.62E-10	1.69E-08	1.83E-07	1.32E-08	3.77E-08	3.44E-07	4.37E-08	7.04E-08	9.56E-08	1.37E-07	1.06E-07	4.66E-08	3.42E-08	1.06E-08	2.53E-04	4.05E-08	1.78E-08	1.78E-08	1.78E-08	1.78E-08	3.63E-07	8.53E-10	1.61E-08	2.25E-09	4.13E-09	1.07E-08	3.60E-07
Red Marrow	6.85E-08	2.75E-08	1.57E-08	2.79E-08	5.67E-08	4.86E-08	2.08E-08	3.91E-08	3.03E-08	3.03E-08	4.74E-08	2.31E-08	3.07E-08	2.53E-08	5.78E-08	3.87E-08	1.19E-05	5.60E-08	4.32E-06	5.60E-08	2.48E-06	2.34E-08	7.48E-09	2.29E-08	2.19E-08	2.19E-08	3.76E-08	2.67E-07
Osteogenic Cells	6.88E-08	7.85E-08	2.00E-08	2.71E-08	4.59E-08	3.61E-08	2.50E-08	3.10E-08	3.90E-08	3.90E-08	4.07E-08	3.07E-08	4.24E-08	4.68E-08	4.18E-08	4.13E-08	5.58E-06	1.33E-05	1.70E-05	3.17E-06	8.17E-06	3.14E-08	2.44E-08	3.11E-08	4.95E-08	2.49E-08	3.10E-08	1.08E-06
Skin	9.53E-09	1.16E-08	2.15E-08	8.79E-09	1.00E-08	8.36E-09	9.58E-09	8.79E-09	9.58E-09	1.05E-08	1.11E-08	1.02E-08	1.13E-08	1.63E-08	8.70E-09	8.36E-09	1.21E-08	1.37E-08	1.37E-08	1.37E-08	1.37E-08	1.01E-08	2.94E-08	1.28E-08	1.27E-08	1.11E-08	8.36E-09	3.36E-07
Spleen	1.26E-07	2.24E-10	1.25E-08	3.41E-08	1.66E-08	2.70E-08	2.15E-07	2.74E-08	3.24E-08	4.39E-08	1.85E-07	1.97E-08	4.52E-08	2.87E-08	1.06E-08	3.63E-07	2.48E-08	1.35E-08	1.35E-08	1.35E-08	1.35E-08	1.31E-04	7.14E-10	9.53E-09	2.33E-09	2.69E-09	7.25E-09	3.54E-07
Testes	5.20E-10	7.62E-13	0.00E+00	2.14E-09	3.95E-08	7.00E-09	9.96E-10	5.70E-09	1.87E-10	2.23E-10	1.05E-09	5.30E-10	1.35E-10	2.77E-08	0.00E+00	8.53E-10	8.51E-09	1.13E-08	1.13E-08	1.13E-08	1.13E-08	7.14E-10	6.10E-04	7.43E-11	1.04E-11	1.05E-07	0.00E+00	3.47E-07
Thymus	1.61E-08	2.19E-09	6.75E-08	4.20E-09	6.68E-10	1.48E-09	1.04E-08	1.74E-09	2.47E-07	2.04E-07	5.08E-09	1.61E-08	7.75E-08	2.94E-08	6.56E-10	1.61E-08	2.35E-08	1.34E-08	1.34E-08	1.34E-08	1.34E-08	9.53E-09	7.43E-11	1.14E-03	4.26E-08	2.85E-10	6.11E-10	3.51E-07
Thyroid	2.24E-09	3.69E-08	8.01E-09	8.10E-10	9.34E-11	1.55E-10	8.68E-10	2.72E-10	1.33E-08	1.14E-08	1.06E-09	2.60E-09	2.35E-08	3.24E-08	8.84E-11	2.25E-09	2.07E-08	2.10E-08	2.10E-08	2.10E-08	2.10E-08	2.33E-09	1.04E-11	4.26E-08	1.15E-03	3.91E-11	8.34E-11	3.51E-07
Urinary Bladder Wall	2.28E-09	2.82E-12	4.53E-10	1.24E-08	1.37E-07	5.77E-08	5.17E-09	4.31E-08	7.19E-10	6.10E-10	5.61E-09	3.51E-09	4.61E-10	3.86E-08	1.49E-07	4.27E-09	2.45E-08	1.08E-08	1.08E-08	1.08E-08	1.08E-08	2.55E-09	1.05E-07	2.89E-10	3.95E-11	5.74E-05	3.52E-07	3.57E-07
Uterus	5.88E-09	5.77E-12	8.95E-10	3.05E-08	1.42E-07	2.30E-07	1.32E-08	1.07E-07	1.55E-09	1.81E-09	1.72E-08	8.99E-09	1.30E-09	3.94E-08	4.21E-07	1.07E-08	4.16E-08	1.35E-08	1.35E-08	1.35E-08	1.35E-08	7.25E-09	0.00E+00	6.11E-10	8.34E-11	3.42E-07	3.03E-04	3.61E-07
Total Body	3.58E-07	3.45E-07	3.39E-07	6.64E-08	2.22E-07	2.92E-07	1.27E-07	1.86E-07	1.40E-07	3.56E-07	3.54E-07	3.54E-07	3.50E-07	3.48E-07	3.62E-07	3.61E-07	3.53E-07	3.49E-07	3.49E-07	3.49E-07	3.49E-07	3.54E-07	3.47E-07	3.51E-07	3.52E-07	6.74E-08	3.62E-07	3.49E-07

Figure 9. S-factors for ^{177}Lu Adult Male (mGy/MBq.s) [27]

	Adrenals	Brain	Breasts	GB Cont	LLI Cont	SI Cont	StomCont	ULI Cont	HeartCont	Hrt Wall	Kidneys	Liver	Lungs	Muscle	Ovaries	Pancreas	Red Mar.	CortBone	TrabBone	CortBone	TrabBone	Spleen	Thymus	Thyroid	UB Cont	Uterus	TotBody
Adrenals	1.69E-03	2.28E-10	1.67E-08	1.11E-07	1.02E-08	2.83E-08	8.93E-08	3.25E-08	7.67E-08	8.35E-08	2.68E-07	1.44E-07	8.58E-08	3.90E-08	9.13E-09	3.52E-07	7.86E-08	3.81E-08	3.81E-08	3.61E-08	3.81E-08	1.79E-07	1.60E-08	3.24E-09	3.47E-09	9.34E-09	4.60E-07
Brain	2.20E-10	2.04E-05	1.01E-09	1.36E-10	1.51E-11	3.26E-11	1.89E-10	3.89E-11	9.20E-10	7.97E-10	1.11E-10	3.43E-10	2.24E-09	6.17E-09	1.20E-11	2.19E-10	3.46E-08	4.00E-08	4.00E-08	4.00E-08	4.00E-08	3.00E-10	2.45E-09	1.61E-08	4.16E-12	1.34E-11	4.45E-07
Breasts	1.67E-08	1.01E-09	6.67E-05	1.13E-08	1.24E-09	2.69E-09	2.05E-08	3.70E-09	8.85E-08	9.32E-08	6.94E-09	2.48E-08	7.00E-08	1.53E-08	1.18E-09	2.03E-08	1.68E-08	1.09E-08	1.09E-08	1.09E-08	1.09E-08	1.42E-08	9.03E-08	1.09E-08	7.71E-10	1.26E-09	4.38E-07
Gallbladder Wall	1.20E-07	1.38E-10	1.21E-08	2.39E-04	2.85E-08	1.49E-07	1.17E-07	2.69E-07	3.86E-08	4.10E-08	1.21E-07	2.85E-07	2.80E-08	3.85E-08	4.58E-08	2.85E-07	2.79E-08	1.49E-08	1.49E-08	1.49E-08	1.49E-08	5.39E-08	9.54E-09	1.56E-09	1.66E-08	4.78E-08	4.62E-07
LLI Wall	7.01E-09	1.23E-11	1.15E-09	2.31E-08	8.86E-05	2.09E-07	3.12E-08	8.38E-08	2.12E-09	2.64E-09	1.91E-08	6.55E-09	2.31E-09	4.37E-08	4.09E-07	1.60E-08	7.16E-08	2.48E-08	2.48E-08	2.48E-08	2.48E-08	1.82E-08	8.68E-10	1.60E-10	2.01E-07	1.73E-07	4.62E-07
Small Intestine	2.83E-08	3.26E-11	2.69E-09	1.53E-07	2.42E-07	3.20E-05	7.19E-08	4.27E-07	7.25E-09	8.19E-09	7.50E-08	4.04E-08	6.54E-09	3.83E-08	3.17E-07	5.17E-08	5.90E-08	1.95E-08	1.95E-08	1.95E-08	1.95E-08	3.69E-08	2.28E-09	3.90E-10	7.62E-08	2.81E-07	4.59E-07
Stomach Wall	9.44E-08	2.16E-10	2.20E-08	1.07E-07	4.71E-08	7.49E-08	5.26E-05	1.05E-07	6.36E-08	9.73E-08	7.79E-08	5.93E-08	4.48E-08	3.70E-08	2.32E-08	4.18E-07	2.43E-08	1.47E-08	1.47E-08	1.47E-08	1.47E-08	2.34E-07	1.62E-08	2.39E-09	7.14E-09	2.00E-08	4.59E-07
ULI Wall	3.20E-08	3.87E-11	4.34E-09	2.66E-07	1.05E-07	4.72E-07	9.26E-08	5.72E-05	9.07E-08	1.05E-08	7.02E-08	6.51E-08	7.69E-09	3.41E-08	2.96E-07	6.09E-08	5.01E-08	1.65E-08	1.65E-08	1.65E-08	1.65E-08	3.60E-08	3.11E-09	5.27E-10	5.94E-08	1.50E-07	4.61E-07
Heart Wall	8.36E-08	7.97E-10	9.32E-08	3.96E-08	3.29E-09	8.19E-09	8.67E-08	1.10E-08	2.97E-05	9.96E-05	2.66E-08	8.64E-08	1.58E-07	3.25E-08	3.34E-09	1.15E-07	3.02E-08	1.91E-08	1.91E-08	1.91E-08	1.91E-08	5.53E-08	2.19E-07	1.49E-08	1.19E-09	3.49E-09	4.59E-07
Kidneys	2.68E-07	1.11E-10	6.94E-09	1.23E-07	2.44E-08	7.50E-08	8.05E-08	6.87E-08	2.39E-08	2.66E-08	8.73E-05	9.61E-08	2.63E-08	3.38E-08	2.61E-08	1.65E-07	5.64E-08	2.34E-08	2.34E-08	2.34E-08	2.34E-08	2.29E-07	6.23E-09	1.29E-09	8.46E-09	2.17E-08	4.55E-07
Liver	1.44E-07	3.43E-10	2.49E-08	2.80E-07	7.68E-09	4.04E-08	5.87E-08	6.65E-08	8.12E-08	8.64E-08	9.61E-08	1.77E-05	7.52E-08	2.69E-08	1.46E-08	1.34E-07	2.74E-08	1.72E-08	1.72E-08	1.72E-08	1.72E-08	2.95E-08	2.10E-08	3.81E-09	5.11E-09	1.24E-08	4.56E-07
Lungs	8.67E-08	2.29E-09	7.07E-08	2.66E-08	2.37E-09	6.53E-09	4.29E-08	8.01E-09	1.72E-07	1.61E-07	2.65E-08	7.67E-08	2.99E-05	3.45E-08	2.29E-09	6.59E-08	3.64E-08	2.38E-08	2.38E-08	2.38E-08	2.38E-08	6.11E-08	9.90E-08	3.15E-08	8.94E-10	2.34E-09	4.53E-07
Muscle	3.90E-08	6.17E-09	1.53E-08	3.88E-08	4.16E-08	3.83E-08	3.49E-08	3.68E-08	3.12E-08	3.25E-08	3.38E-08	2.69E-08	3.41E-08	1.42E-06	4.78E-08	4.36E-08	3.10E-08	2.54E-08	2.54E-08	2.54E-08	2.54E-08	3.67E-08	3.70E-08	3.19E-08	4.40E-08	4.78E-08	4.47E-07
Ovaries	9.18E-09	1.20E-11	1.18E-09	4.35E-08	4.64E-07	3.17E-07	2.24E-08	2.61E-07	2.76E-09	3.34E-09	2.61E-08	1.46E-08	2.20E-09	4.78E-08	2.16E-03	1.85E-08	7.13E-08	2.22E-08	2.22E-08	2.22E-08	2.22E-08	1.40E-08	1.03E-09	1.30E-10	1.88E-07	5.52E-07	4.63E-07
Pancreas	3.52E-07	2.19E-10	2.08E-08	2.38E-07	2.04E-08	5.17E-08	4.10E-07	6.14E-08	9.03E-08	1.15E-07	1.65E-07	1.34E-07	6.52E-08	4.36E-08	1.85E-08	2.81E-04	4.20E-08	2.21E-08	2.21E-08	2.21E-08	2.21E-08	4.38E-07	1.88E-08	2.85E-09	5.05E-09	1.51E-08	4.63E-07
Red Marrow	7.79E-08	3.74E-08	1.68E-08	3.05E-08	7.19E-08	5.73E-08	2.38E-08	4.63E-08	3.10E-08	2.95E-08	5.55E-08	2.68E-08	3.53E-08	3.10E-08	7.08E-08	4.11E-08	1.05E-05	6.81E-08	4.51E-06	6.81E-08	2.63E-06	2.86E-08	2.44E-08	2.48E-08	2.82E-08	5.19E-08	3.30E-07
Osteogenic Cells	8.75E-08	9.53E-08	2.46E-08	3.42E-08	5.65E-08	4.56E-08	3.34E-08	3.93E-08	4.62E-08	4.41E-08	5.26E-08	4.08E-08	5.42E-08	5.68E-08	5.20E-08	5.11E-08	7.53E-06	1.77E-05	2.27E-05	4.20E-06	1.09E-05	4.15E-08	3.79E-08	5.61E-08	3.12E-08	3.97E-08	1.46E-06
Skin	1.18E-08	1.39E-08	2.54E-08	1.03E-08	1.23E-08	1.05E-08	1.21E-08	1.05E-08	1.25E-08	1.28E-08	1.35E-08	1.27E-08	1.31E-08	1.93E-08	1.04E-08	1.04E-08	1.52E-08	1.72E-08	1.72E-08	1.72E-08	1.72E-08	1.22E-08	1.59E-08	2.98E-08	1.37E-08	1.08E-08	4.34E-07
Spleen	1.79E-07	3.00E-10	1.40E-08	4.93E-08	2.09E-08	3.69E-08	2.40E-07	3.65E-08	4.19E-08	5.53E-08	2.29E-07	2.95E-08	6.04E-08	3.67E-08	1.40E-08	4.38E-07	2.93E-08	1.79E-08	1.79E-08	1.79E-08	1.79E-08	1.60E-04	1.19E-08	3.04E-09	4.36E-09	1.10E-08	4.56E-07
Thymus	1.60E-08	2.45E-09	9.08E-08	1.00E-08	1.07E-09	2.22E-09	1.43E-08	2.41E-09	2.59E-07	2.19E-07	6.23E-08	2.10E-08	9.71E-08	3.70E-08	1.03E-09	1.88E-08	2.48E-08	1.65E-08	1.65E-08	1.65E-08	1.65E-08	1.19E-08	1.19E-03	6.85E-08	4.99E-10	9.77E-10	4.53E-07
Thyroid	3.24E-09	1.61E-08	1.09E-08	1.56E-09	1.98E-10	3.90E-10	2.26E-09	5.24E-10	1.92E-08	1.49E-08	1.29E-09	3.81E-09	3.13E-08	3.19E-08	1.30E-10	2.85E-09	2.51E-08	2.39E-08	2.39E-08	2.39E-08	2.39E-08	3.04E-09	6.85E-08	1.40E-03	8.20E-11	1.77E-10	4.46E-07
Urinary Bladder Wall	3.75E-09	5.98E-12	8.77E-10	1.92E-08	1.63E-07	7.99E-08	6.86E-09	5.62E-08	1.42E-09	1.53E-09	1.01E-08	5.37E-09	9.83E-10	5.19E-08	1.86E-07	5.82E-09	2.82E-08	1.44E-08	1.44E-08	1.44E-08	1.44E-08	4.63E-09	5.08E-10	8.35E-11	7.60E-05	4.01E-07	4.59E-07
Uterus	9.34E-09	1.34E-11	1.26E-09	4.20E-08	1.91E-07	2.81E-07	2.07E-08	1.41E-07	2.91E-09	3.49E-09	2.17E-08	1.24E-08	2.33E-09	4.78E-08	5.52E-07	1.51E-08	5.19E-08	1.70E-08	1.70E-08	1.70E-08	1.70E-08	1.10E-08	9.77E-10	1.77E-10	4.12E-07	2.99E-04	4.62E-07
Total Body	4.62E-07	4.44E-07	4.39E-07	7.73E-08	2.80E-07	3.75E-07	1.64E-07	2.40E-07	1.58E-07	4.54E-07	4.57E-07	4.57E-07	4.53E-07	4.43E-07	4.64E-07	4.65E-07	4.54E-07	4.50E-07	4.50E-07	4.50E-07	4.50E-07	4.53E-07	4.52E-07	4.48E-07	8.58E-08	4.64E-07	4.49E-07

Figure 10. S-factors for ^{177}Lu AdultFemale (mGy/MBq.s) [27]

Target Organ	Mass (g)
Adrenals	1.63E+01
Brain	1.42E+03
Breasts	3.51E+02
Gallbladder Wall	1.05E+01
LLI Wall	1.67E+02
Small Intestine	6.77E+02
Stomach Wall	1.58E+02
ULI Wall	2.20E+02
Heart Wall	3.16E+02
Kidneys	2.99E+02
Liver	1.91E+03
Lungs	1.00E+03
Muscle	2.80E+04
Ovaries	8.71E+00
Pancreas	9.43E+01
Red Marrow	1.12E+03
Osteogenic Cells	1.20E+02
Skin	3.01E+03
Spleen	1.83E+02
Testes	3.91E+01
Thymus	2.09E+01
Thyroid	2.07E+01
Urinary Bladder Wall	4.76E+01
Uterus	7.90E+01
Total Body	7.37E+04

Figure 11. Mass of organs in Adult Male phantom [27].

Target Organ	Mass (g)
Adrenals	1.40E+01
Brain	1.20E+03
Breasts	3.60E+02
Gallbladder Wall	8.00E+00
LLI Wall	1.60E+02
Small Intestine	6.00E+02
Stomach Wall	1.40E+02
ULI Wall	2.00E+02
Heart Wall	2.40E+02
Kidneys	2.75E+02
Liver	1.40E+03
Lungs	8.00E+02
Muscle	1.70E+04
Ovaries	1.10E+01
Pancreas	8.50E+01
Red Marrow	1.30E+03
Osteogenic Cells	9.00E+01
Skin	1.79E+03
Spleen	1.50E+02
Thymus	2.00E+01
Thyroid	1.70E+01
Urinary Bladder Wall	3.59E+01
Uterus	8.00E+01
Total Body	5.69E+04

Figure 12. Mass of organs in Adult Female phantom [27]

Discussion

In most developing countries planar imaging is often the only means of performing dosimetry. Although not as accurate as single photon emission computed tomography (SPECT)/CT quantification dosimetry, planar quantification dosimetry provides an advantage in cases when whole body uptake is of interest through axial coverage [21]. The basic knowledge of planar quantification is also a method that can be used for dosimetry teaching purposes and may be used as a quality control tool to verify counts in particular organs, as demonstrated by results in this study.

The Masterdose design is a multiplatform tool, which runs on any Windows, Linux and Macintosh platform. Each UI on Masterdose was tested against hand calculations by the authors, ensuring correctness. Compared with the effects of scatter, the effects of attenuation are larger in magnitude [6]. The use of a *gAFC* represents a unique option by Masterdose software, studies have shown that without any attenuation correction, organ dose results may be inadequate with an error as large as ±60% [21-23]. Masterdose software allows users to enter attenuation, scatter and "counts to activity" correction factors performed by the medical physicist, for each collimator, gamma energy and energy window setting used by a specific hospital. This feature allows medical physicists to use Masterdose software for dosimetry quantification of various therapeutic isotopes at multiple hospitals. One challenge experienced, however, was placing the scatter energy windows on the Philips Marconi Meridian gamma camera, due to the gamma camera's age. The authors needed assistance from the manufacturer for this. The Masterdose software allows for planar dose determination of the kidneys and liver. The generation of a PDF file and print option also further assists with therapeutic planning of the patient.

Masterdose software was designed to not limit the number of images that may be uploaded for time-point calculations. Time-points may be generated a few hours after the injection, one day after, close to the effective half-life of the therapeutic isotope or three times the effective half-life, allowing for customized determination of the molecular time-integrated activity coefficients.

The Masterdose software was validated against OLINDA/EXM [27]. Our software seamlessly accepts planar images from gamma cameras, and there is the capability for user to zoom images, which aids in the drawing of ROI. All ROI was corrected for background, attenuation and scatter as demonstrated from this study. To maintain the accuracy of the ROI, it was drawn on the first image of a patient and copied to subsequent patient images. A limitation of the Masterdose software, however, is that it cannot load PET co-registered with CT images. Also, not part of the software's ability is the correction for ROI overlap. Both these limitations will be addressed in the next version of the Masterdose software.

In conclusion, Masterdose software is an option that can be used for planar dosimetry in developing countries due to its multi-task platforms that allows for quantification of any therapeutic isotope. The software can be used to track accumulative doses for different patient therapeutic cycles, limiting dose to organs at risk such as the kidneys and liver, whilst optimizing tumour doses. Masterdose also has the ability of being used for multi-center dosimetry.

Acknowledgement

The authors would like to express their sincere gratitude to the nuclear medicine departments at Witwatersrand University-Donald Gordon Medical Centre and Inkosi Albert Luthuli Central Hospital.

Special thanks go to Monageng Motsabi for assisting with and "fine-tuning" the Masterdose software, and from who the name of the software probably comes from, due to us calling each other "Master".

A special thanks also to Thulani Nyathi who is always willing to provide valuable critic to any manuscript that the first author writes.

Funding

Sincere gratitude to the research department at Sefako Makgatho University for making funding available for the research.

Ethical approval

Sefako Makgatho Health Sciences University Research Ethics Committee approved this study, SMUREC Ethics Reference Number: SMUREC//M/114/2018: PG

Authors' contribution

Bronwin Van Wyk developed Masterdose, analyzed and interpreted manuscript findings; Francis Hasford, Nozipho Nyakale and Mboyo-Di-Tamba Vangu interpreted and supervised the manuscript findings. All authors read and approved the final version of the manuscript.

The authors declare that they have no conflicts of interest.

Bibliography

1. Quantitative nuclear medicine imaging: concepts, requirements and methods. Vienna: International Atomic Energy Agency, 2014. IAEA human health series, ISSN 2074-7667; no. 9
2. Frey EC, Humm JL, Ljungberg M. Accuracy and precision of radioactivity quantification in nuclear medicine images. *Semin Nucl Med* 2012; 42(3): 208-18.
3. Ljunberg M, SjogreenGleiser K. Personalized dosimetry for radionuclide therapy using molecular tools. *Biomedicines* 2016; 4: 25.
4. Sjogreen-Gleiser K, Dewaraja YK, Chiesa C. Dosimetry in patients with B-cell lymphoma treated with [^{90}Y]libritumomabtiuxetan or [^{131}I]tositumomab. *Q J Nucl Med Mol Imaging* 2011; 55:126.
5. He B, Wahl RL, Du Y et al. Comparison of residence time estimation methods for radioimmunotherapy dosimetry and treatment planning-Monte Carlo simulation studies. *IEEE Trans Med Imaging* 2008; 27: 521-30.
6. Sjogreen Gleisner K. Scatter correction by deconvolution of planar whole-body scintillation camera images using an image-based estimate of the signal-to-noise ratio. *Eur J Nucl Med* 2012; 39: S304-53.
7. Li T, Zhu L, Lu Z et al. BIGDOSE: software for 3D personalized targeted radionuclide therapy dosimetry. *Quant Imaging Med Surg* 2020; 10(1): 160-70.

8. Hippeläinen ET, Tenhunen MJ, Maenpaa HO et al. Dosimetry software Hermes Internal Radiation Dosimetry: from quantitative image reconstruction to voxel-level absorbed dose distribution. *Nucl Med Commun* 2017; 38: 357-65.
9. Marcatili S,Pettinato C, Daniels S et al. Development and validation of RAYDOSE: a Geant4-based application for molecular radiotherapy. *Phys Med Biol* 2013; 58: 2491-508.
10. Dieudonné A, Aouf A, Sabet A et al. Correlation between average absorbed dose and metabolic response in the radio-embolization of liver colorectal metastases with resin microspheres. *J Nucl Med* 2015; 56: 1237-7.
12. Grassi E, Fioroni F, Ferri V et al. Quantitative comparison between the commercial software STRATOS((R)) by Philips and a homemade software for voxel-dosimetry in radiopeptide therapy. *Phys Med* 2015; 31: 72-9.
13. Jackson PA, Beauregard JM, Hofman MS et al. An automated voxelized dosimetry tool for radionuclide therapy based on serial quantitative SPECT/CT imaging. *Med Phys* 2013; 40:112503.
14. Grimes J, Uribe C, Celler A. JADA: a graphical user interface for comprehensive internal dose assessment in nuclear medicine. *Med Phys* 2013; 40: 072501.
15. Berker Y, Goedicke A, Kemerink GJ et al. Activity quantification combining conjugate-view planar scintigraphies and SPECT/CT data for patient-specific 3-D dosimetry in radionuclide therapy. *Eur J Nucl Med Mol Imaging* 2011; 38: 2173-85.
16. Kost SD, Dewaraja YK, Abramson RG, Stabin MG. VIDA: a voxel-based dosimetry method for targeted radionuclide therapy using Geant 4. *Cancer Biother Radiopharm* 2015; 30: 16-26.
17. Ramos SMO, Thomas S, Pinheiro MA et al. Internal radiation dose and modeling codes in nuclear medicine: A fresh look at old problems. *Int J Radiol Radiat Ther* 2017; 4: 439-43.
18. https://rsdphantoms.com/radiation-therapy/the-alderson-radiation-therapy-phantom. Radiology support devices Inc. Accessed 27 December 2020.
19. Petitguillaume A, Bernardini M, Broggio D et al. OEDIPE, a software for personalized Monte Carlo dosimetry and treatment planning optimization in nuclear medicine: absorbed dose and biologically effective dose considerations. *Radioprotection* 2014; 49: 275-81.
20. National Electrical Manufacturers' Association (NEMA): Standard Publication NU 1-2001. Performance Measurements of Scintillation Cameras. Washington: NEMA; 2001.
21. Sjögreen K, Ljungberg M, Wingärdh K et al. The LundADose method for planar image activity quantification and absorbed-dose assessment in radionuclide therapy. *Cancer Biother Radiopharm* 2005; 20(1): 92-7.
22. https://iopscience.iop.org/article/10.1088/1742-6596/694/1/012056/pdf. Development of a software tool for internal dosimetry using MIRD method. Accessed 21/01/2021.
23. https://www.iaea.org/projects/crp/e21007. Development of Quantitative Nuclear Medicine Imaging for Patient Specific Dosimetry. Accessed 21/04/2021.
24. Minarik D, Sjogreen K, Ljungberg M. A new method to obtain transmission images for planar whole-body activity quantification. *Cancer Biother Radiopharm* 2005; 20: 72.
25. International Commission on Radiation Units and Measurements. Report 44: Tissue Substitutes in Radiation Dosimetry and Measurement. Bethesda, MD: ICRU; 1989.
26. https://www.nist.gov/pml/data/photon_cs. Bibliography of Photon Total Cross Section (Attenuation Coefficient) Measurements (version 2.3). National Institute of Standards and Technology; 2003. Accessed on 18 August 2020.
27. Stabin MG, Sparks RB, Crowe E. OLINDA/EXM: The Second-Generation Personal Computer Software for Internal Dose Assessment in Nuclear Medicine. *J Nucl Med* 2005; 46: 1023-7.
28 .https://inis.iaea.org/search/search.aspx?orig_q=RN:44078412. Sensitivity comparative study in Philips Forte Gamma Camera. Accessed 10/10/2021.